9

Mass Transfer Within the Location Where Micro Electroplating Takes Place

Jing-Chie Lin[1], Ting-Kang Chang[2],
Jen-Horn Yang[2], Yean-Ren Hwang[3] and Chuan Li[4]
[1]*Institute of Materials Science and Engineering, National Central University,*
[2,3,4]*Department of Mechanical Engineering, National Central University,*
Taiwan

1. Introduction

Electroplating and electroforming are the two electrochemical processes extensively used in metal fabrication. Electroplating provides a thin metal film to bestow the surface with desired property such as abrasion and wear resistance, corrosion protection, lubricity and aesthetic qualities; electroforming leads to a deposition of metal skin onto a mandrel which is then removed and then the metal deposit was thickened to obtain precise fabrication of molds. Both the electrochemical processes are carried out in the bath where sufficient concentration of metal salt is supplied in presence of an electric field. The electrochemical kinetics is determined not only by the strength of electric field but also by the mass transport phenomenon of the electrochemical active ions. The electric field employed in the electroplating is relatively lower and the field distribution is homogeneous. In contrast, the electrical field exerted in electroforming seems to be much stronger and the field distribution becomes less homogeneous.

In 1995, a novel localized electrochemical deposition (LECD) process was pioneered by Hunter [1] to fabricate three-dimensional (3D) metal microstructures. The LECD brings the electrochemical process to a new era. However, in the LECD process, the electrical field exerted at the electroplating site is super high and the distribution of field strength is ultra heterogeneous. The phenomenon of mass transport in such a strong field distributed in extremely heterogeneous is the case which we have never encountered in doing usual electrodeposition. In the process of micro electroplating, the site where LECD taking place was experimentally controlled to along the track guided with a microanode. Accordingly, the micro metallic features could be fabricated electrochemically along the motional track guided by the microanode [2]. Due to this fact, LECD was also named as microanode guided electroplating (MAGE) process. The schematic diagram of MAGE is shown in Fig. 1.

A platinum wire (diameter in the range from 25 to 125 μm) was fixed coaxially, and cold mounted with epoxy resin in polymethylmethacrylate (PMMA) tube (inner and outer diameters are 3 and 5 mm, respectively) to expose a disk (25 ~ 125 μm in diameter) acting as the microanode. The micranode was driven to move by a stepping motor in an electroplating bath thus guiding the micro electroplating way according to the program built in the micro-CPU. The micoanode assembly and microanode was driven to move by a

stepping motor under precise control, as shown in Fig. 1. In Fig. 1, the cathode was placed horizontally in the electrolytic cell (F) and connected with the negative pole of the dc power supply (V). The microanode assembly (H), connected with the positive pole of the power supply (V), was vertically fixed on a one-dimensional moving table. A servo micro-stepping motor (M) was used to drive the table through a micro-CPU (C) via the D/A converter (D) and driver (E). A relay (G) was connected with the anode assembly. Through control with dedicated software, the microanode was moved vertically with a resolution of 20 nm per step. Prior to electroplating, intimate contact between the microanode and the cathode was assured through a measurement of null electrical resistance. The microanode was then lifted from the cathode to a variety of gaps (in the range from 1 to 100 μm) to start the MAGE. In this study, a variety of dc-voltage biases (in the range from 3 to 6 V) were employed to conduct MAGE and their corresponding current was monitored with the current sensor (A).

So far we have publish a few papers [2-11] to discuss the electrochemical kinetics with respect to MAGE process. The heterogeneous distribution of very intensive electric field in local sites was determined significantly by experimental parameters such as motion modes of the microanode, applied electric voltage, initial gap between the cathode and microanode, and etc. In the present work, we concentrate ourselves on mass balance of electrochemical active ions those which supplied via mass transport from the bulk solution and to be consumed to turn into metallic micro feature. In terms of various models, we applied the commercial software ANSYS 8.0 to simulate the systems so as to understand the electrochemical mechanism of the MAGE process.

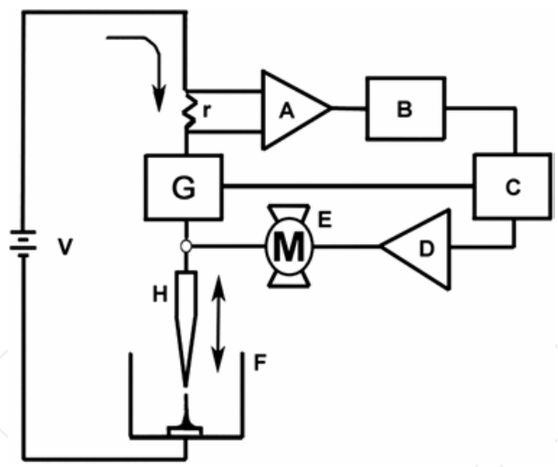

Fig. 1. Schematic diagram of the microanode-guide electroplating system in which the capital letters denote the following. (A) Current sensor, (B) A/D converter, (C) micro-CPU, (D) D/A converter, (E) driver, (F) cell, (G) relay, (H) anode,(M) micro-stepping motor and (V) voltage source

2. Surface morphology of micrometer columns influenced by motion modes of the micro anode

At first, the morphology of micrometer columns fabricated in nickel sulfate bath by MAGE was of concern interest. Optical microscopy (OM) and scanning electron microscopy (SEM,

S3500, Hitachi Co.) were employed to observe their surface morphology. Figure 2 depicts the OM of the micro columns fabricated under certain conditions with different motion modes of the micro anode. As the micro anode was driven to ascend continuously at a constant rate of 1.8 μm s^{-1} to perform MAGE at 5.0 V, a column appearing in dendrite was formed (Fig. 2(a)). In contrast, if the micro anode was driven to ascend intermittently (with an initial gap of 10 μm within each intermittent cycle) at the same voltage (i.e., 5.0 V) until reaching certain heights, a column revealing periodical nodes (Fig. 2(b)) was established. Comparing with both the columns, we found that they showed a similar diameter (roughly 50 μm), the dendrite tended to decrease the diameter with increasing its height, as shown in Fig. 2(a); however, the nodal one, depicted in Fig. 2(b), tended to vary the diameter periodically with the height. If we conducted the intermittent MAGE under a lower bias (i.e., at 3.5 V), we obtain a micrometer nickel column in uniform diameter (50 μm) with smooth morphology (as shown in Fig. 2(c)).

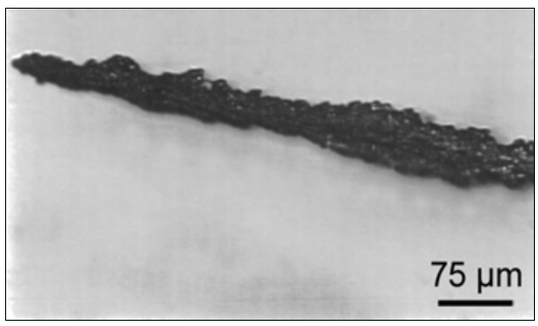

(a)

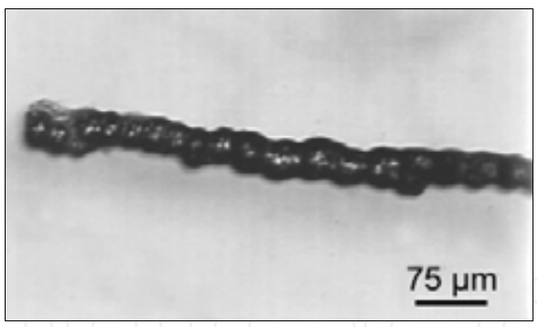

(b)

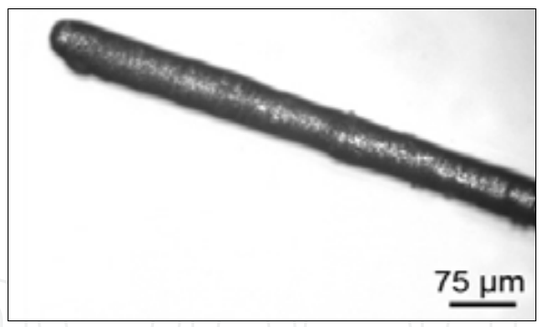

(c)

Fig. 2. Optical micrographs (OM) of the nickel micrometer columns fabricated by the MAGE process in a sulfate bath where the initial gap between the electrodes was the same (at 10 μm) but their dc-voltage bias and the motion mode of the microanode changed as follows: (a) bias at 5.0 V and the microanode moved continuously at a rate of 1.8 μm s^{-1}, (b) bias at 5.0 V and the microanode moved intermittently and (c) bias at 3.5 V and the microanode moved intermittently

Figure 3(a) exhibits SEM morphologies of a nickel column consisting of two segments due to change of voltages in the intermittent MAGE. With respect to fabricating the lower segment (i.e., 3(b) in Fig. 3(a)), we conducted MAGE at 3.2 V until reaching a height of 500 μm. Then we switched the voltage to 4.0 V to continue the MAGE process to grow the upper segment

(i.e., 3(c) in Fig. 3(a)) up to 1000 μm. In higher magnification, we are able to distinguish between Fig. 3(b) and (c). The upper segment is covered by greater (65 μm in diameter) nodular particles but the lower one is covered by finer particles (44 μm in diameter). The deviation of particle sizes is higher for the upper (±3.5 μm) than the lower (±0.5 μm).

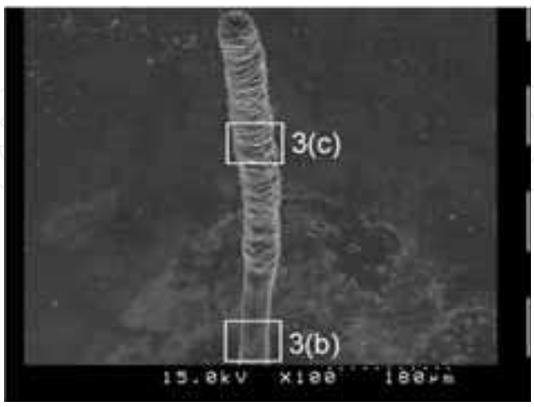

(a)

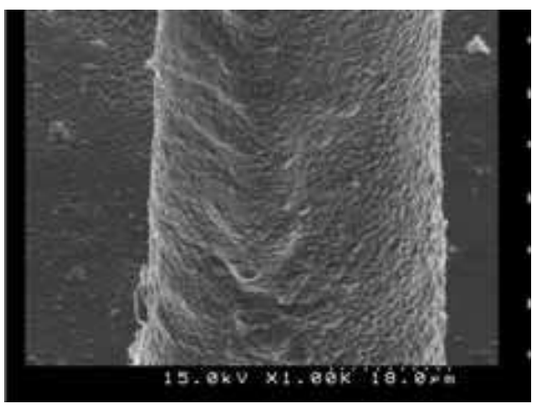

(b)

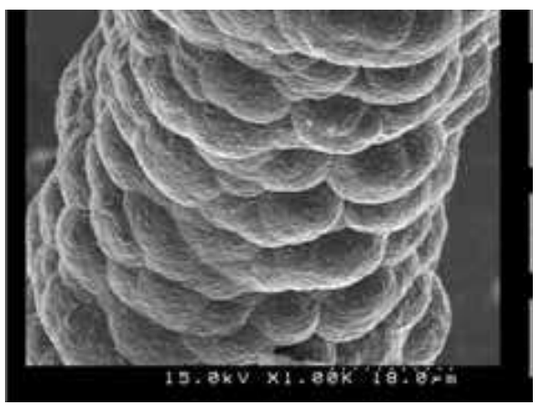

(c)

Fig. 3. (a) SEM morphology of the nickel microcolumn resulted from intermittent MAGE under two different biases in a sulfate bath where the microanode was kept at a separation of 10 μm from the cathode to start electroplating in each step. The microcolumn was deposited at a bias of 3.2 V on the copper surface to a height of 500 μm, then the bias was switched to 4.0 V to continue the deposition from 500 to 1000 μm. (b) Magnified morphology of the lower portion (formed at a bias of 3.2 V) and (c) Magnified morphology of the upper portion (formed at a bias of 4.0 V) for the micrometer nickel column

3. Current measured in the continuous MAGE

Figure 4 exhibits the variation of electroplating current against time in MAGE process where the microanode was ascended continuously at a constant rate of 2.0 μm s^{-1}. In Fig. 4, we found that continuous MAGE could only possibly be performed in the voltage range from 3.0 to 5.0 V. Otherwise, as the continuous MAGE is conducted at voltages less than 2 V, the current responsible for growing the column is too tiny (in a range from 325 to 25 μA) to be

used in practice. To the contrary, as the continuous MAGE is performed at voltages higher than 6.0 V, the current rose rapidly (in 18 s) to reach a critical value (i.e., 20mA), then the circuit is shut off on the purpose to protect the apparatus. As shown in Fig. 4, the current rises fast and it fluctuates profoundly with the continuous MAGE conducted at higher voltages (e.g., 4 and 5 V) than at lower voltages (e.g., 3 V). Higher current may result from abundant reduction of nickel ions and hydrogen ions; current fluctuation especially happened at higher voltages is ascribed to gas –bubbling (evolution of oxygen and hydrogen gas) from both electrodes.

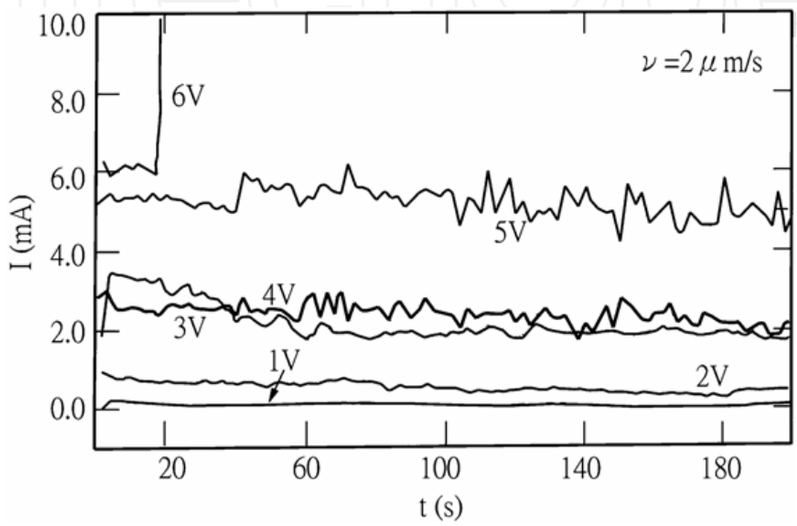

Fig. 4. A plot of current against the electroplating time for the MAGE process conducted at various biases and the microanode moved continuously at a constant rate (e.g., 2.0 μm s^{-1}). The initial gap between the microanode and the Cu-substrate was 20 μm

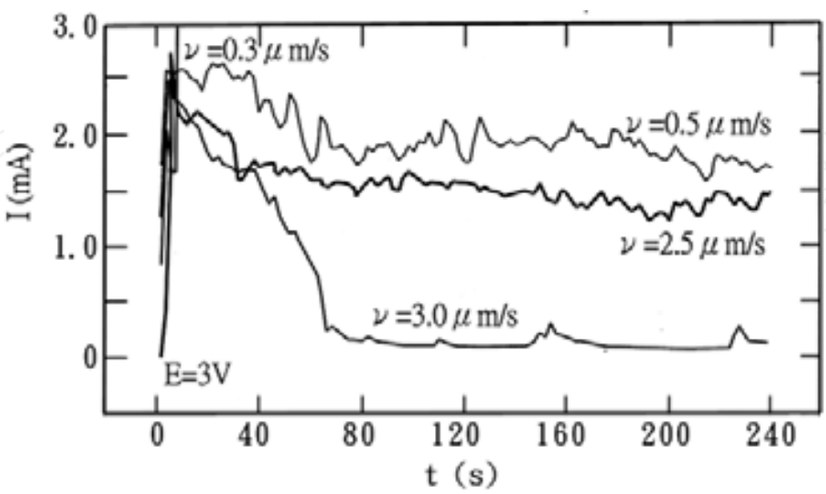

Fig. 5. Current against the electroplating time in the process of continuous MAGE at a bias of 3.0 V with the motion rate of the microanode varying in the range from 0.3 to 3.0 μm s^{-1}. The initial gap between the microanode and the Cu-substrate was 20 μm

Another plot is given in Fig. 5 to show the current variation against time for MAGE conducted at 3.0 V by controlling the microanode to ascend continuously at a variety of rates from 0.3 to 3.0 μm s^{-1}. In Fig. 5, on the curve responsible for continuous MAGE with ascending rate at 3.0 μm s^{-1}, the current rises abruptly to 2.5 mA, drops to 0.25 mA in 60 s and levels off subsequently. This implies that the nickel column grows very fast in the initial period (less than 60 s) but the growth rate in the subsequent stages decays to very slow. Even the duration of this process lasted for 240 s, the column grew rapidly to a height of 25.1 μm almost within the initial 60 s. In contrast to the case where the microanode ascended continuously at 0.3μm s^{-1}, the current led to a sudden rise in 10 s. The growth rate of the column is much faster than the ascending rate of the microanode. As a result, the column grows so swiftly that facilitates its top to contact the microanode. This short-circuit contact may ruin the apparatus. Therefore, on purpose to protect the apparatus, we designed an automatic switch into the system. Once the current exceeding 20 mA the power of the system is shut off. According to Fig. 5, the ascending rate of the microanode is better controlled in the range from 0.5 to 2.0 μm s^{-1} to ensure longer duration for column growth.

4. Current measured in the intermittent MAGE

Figure 6 demonstrates the current variation with time for the intermittent MAGE conducted at 3.2 and 4.2 V, respectively. The initiate gap between the electrodes was set at 10 μm in each intermittent cycle. Two different time-intervals are concerned: within the initial 20 s, the current profile is displayed in Fig. 6(a); at the final stage to grow a column up to 500 μm, the current profile is shown in Fig. 6 (b). The current exhibits different profiles in Fig. 6(a) depending upon the voltages employed. The current level responsible for on-time intermittent MAGE conducting at 4.2 V is higher than that conducting at 3.2 V (i.e., −3.70 ± 0.19 mA as compared to −2.26 ± 0.07 mA); however, the time period at 4.2 V is shorter than that at 3.2 V (i.e., 0.24–0.95 s against 6.19–8.81 s). Greater current variation is also found at 4.2 V than 3.2 V.

Analysis of the current profile in the initial 20 s indicates that intermittent MAGE conducted at 4.2 V almost completing 10 cycles (each cycle including one on-time half cycle and off-time half cycle) but that conducted at 3.2 V only accomplishing 2.3 cycles. Total height of the micrometer column could be estimated from multiplication of the intermittent gap (i.e., 10 μm per cycle) with the number of off-time cycles (i.e., the height roughly at 100 μm for 4.2 V compared to 23 μm for 3.2 V). Checking with SEM examination, the columns fabricated by intermittent MAGE at 4.2 and 3.2 V revealed their heights at 93 and 22 μm, respectively. Obviously, the intermittent MAGE conducted at 3.2 V revealed better consistency for the column height coming from calculated and observed results.

It is possible to evaluate the time needed to grow a nickel microcolumn up to 500 μm. Fig. 6 (b) displays a few final cycles in the cases of intermittent MAGE conducted at 4.2V (on the left-hand side) and at 3.2V (on the right-hand side), respectively. It takes 107.18 s (overall *t*-on = 35.78 s; overall *t*-off = 71.40 s) at 4.2 V, and 510.03 s (overall *t*-on=438.63; overall *t*-off=71.40 s) at 3.2 V, respectively. If time-consumption for ascending the microanode is ignored, the average growth rates are estimated at 13.97 and 1.14 μm s^{-1} for the columns fabricated by intermittent MAGE conducted at 4.2 and 3.2 V, respectively. A close examination in Figs 6(a) and (b) indicated that the off-time period is a constant (1.4 s) but the on-time period varies with voltages employed.

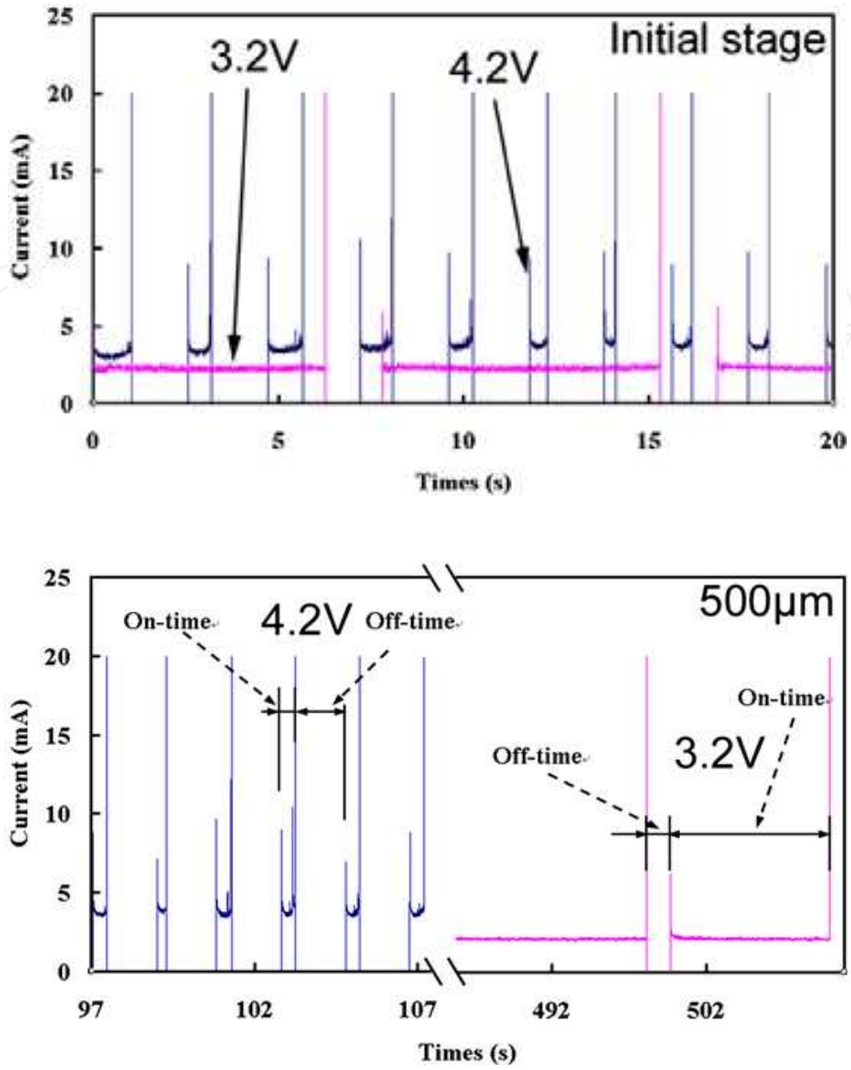

Fig. 6. Variation of current with the electroplating time for the micrometer nickel column fabricated via intermittent MAGE at 3.2 and 4.2 V during (a) the initial stage (in 20 s) and (b) the final stage to reach a column height of 500 μm. The initial gap is at 10 μm in each intermittent cycle

5. Models for column growth in continuous MAGE

A schematic model is demonstrated in Fig. 7(a) to illustrate the growth of the column fabricated by continuous MAGE. Prior to electrochemical reaction, the microanode was ascended to keep an initial gap of 20 μm from the cathode. As soon as the electrochemical deposition started, the microanode was driven to ascend at a constant rate (V). In response to stages 1, 2, ... and n, as shown in Fig. 7(a1), (a2) and (a3), the micrometer column was growing to various heights (i.e., at h_1, h_2, ... and h_n) with the separation between the microanode and microcolumn at d_1, d_2, ... and d_n, respectively. The dashed region in Fig. 7(a3) was re-plotted in Fig. 7(an) for detailed investigation. Supposedly a column established continuously from the (n-1)th stage to nth. The top surface of the column

established at the (n-1)th stage was covered by new deposit coming from the nth stage. It is well known that both deposition rate and surface coverage are determined by the strength of electric field exerted. Accordingly, at the instance of (n-1) stage, the strength at the center top of the column is the strongest, this strength decreases from the center to periphery at the column transverse. Under the condition where the strength of $E_{(n-1)}$ is small enough, no contribution of deposition leads to a confinement of maximal radius at $R_{(n-1)}$ for the column. In the continuous MAGE process, the variation of strength may depend upon the ascending rate of the microanode. Under higher ascending rates, the microanode moves further away from the column in shorter durations. The separation between the microanode and the microcolumn tends to increase in the sequence 20μm < d1< d2 < dn, so that the electric field strength reduces rapidly with time. A field gradient between E_n and $E_{(n-1)}$ caused by this quick strength change will be intensified and the strength of $E_{(n-1)}$ is soon reduced to an insignificant magnitude. Further proceeding to the process at the nth stage, the deposition would undergo mainly on the top rather than on the periphery of the column. As a result, the columns fabricated by continuous MAGE tended to reduce their radius gradually thus exhibiting the dendrite morphology as shown in Fig 2 (a). The strength difference between the (n-1)th and nth stages may offer an indication of radius uniformity for the column. It is defined by ΔE^c in Eq (5.1)

$$\Delta E^c = E_n - E_{(n-1)} \tag{5.1}$$

Where $E_{(n-1)}$ and E_n denote the strength at the (n-1) and nth stages, respectively. Moreover, the mean strength (E_m^c) defined in Eq (5.2), also based on the strengths arisen from the (n-1)th and nth stages

$$E_m^c = [E_{(n-1)} + E_n]/2 \tag{5.2}$$

Both the ΔE^c and E_m^c provide with a criterion to judge whether the microcolumn is possible to grow.

In the case of continuous MAGE conducted at higher voltages under lower ascending rate of the microanode, the strength gets stronger resultant from the growth of the column to diminish the gap between the electrodes. If the growth rate on the column is much higher than the ascending rate of the microanode, the separation between the microanode and the microcolumn will deduce in the order 20 μm > d1 > d2 > dn. Increasing with the elapsed time, this gap is soon reduced so that the field strength and the current responsible for electrochemical deposition are both intensified. Once the current measured exceeding 20 mA, the power of this system is shut off to interrupt MAGE for protection. Theoretically, fabrication of a micrometer column to any height is possible by continuous MAGE via optimal controlling the experimental conditions to balance the growth rate of the microcolumn with the ascending rate of the microanode. It may be accomplished by controlling a constant gap between the microanode and the microcolumn (e.g., 20 μm = d1 = d2 = dn) at any time. However, it is not easy to manipulate in practice. The microcolumn exhibited in figure 2(a) is the longest one we had via continuous MAGE.

Figure 7(b) shows a simulated diagram to elucidate the strength distribution for the electric field strength exerted in the continuous MAGE conducted at 5 V for 240 s, under an initial gap of 20 μm, with ascending rate of the microanode at 2 μm s^{-1}. This simulation is accomplished using the commercial software ANSYS 8.0 by input the data of electrical conductivity of electrolyte with 42.02 mS cm^{-1}. According to the same procedure, we also

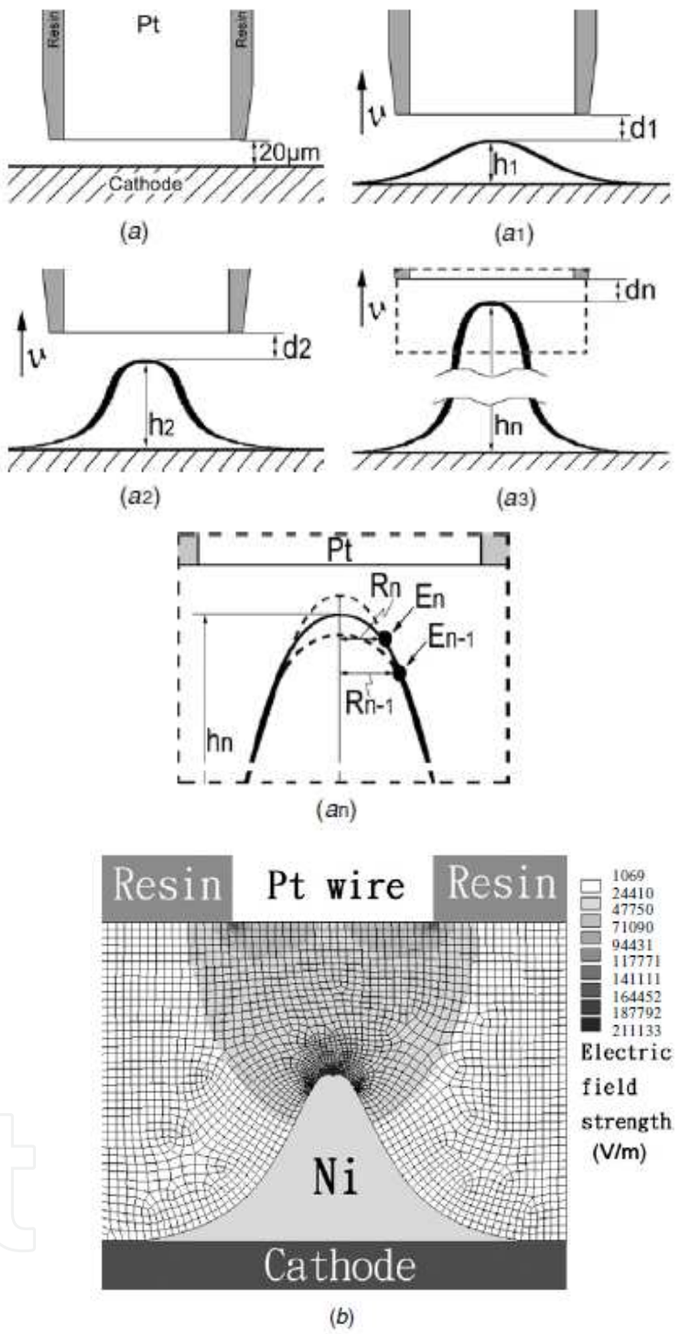

Fig. 7. (a) A scheme of sequential models for the continuous MAGE process initiated with a gap of 20 μm between the microanode and the Cu-substrate. In the diagrams, h_1, h_2, ..., h_n and R_1, R_2, ..., R_n represent the column height and column radius at a variety of duration t_1, t_2...and t_n, respectively. The eventual gaps in response to different duration are d_1, d_2 ... and d_n. The strength of electric-field strength at t_{n-1} and t_n is represented by E_{n-1} and E_n. (b) Distribution map of the electric-field strength simulated with the software ANSYS 8.0 for the system conducted by the continuous MAGE at the final stage. The bias is 5.0 V and the conductivity of the electrolyte is 42.02 mS cm^{-1}

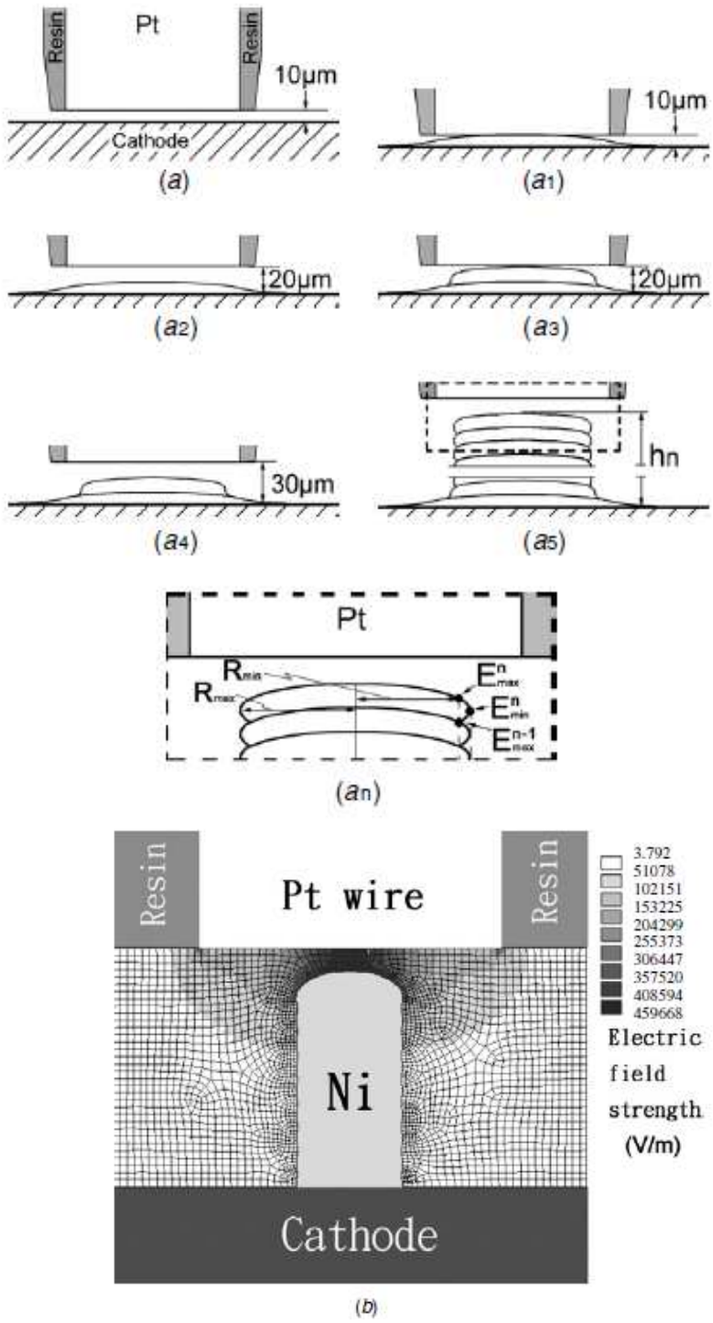

Fig. 8. (a) A scheme of sequential models for the intermittent MAGE process with each cycle initiated with a gap of 10 μm between the microanode and the column top. In the diagrams, h_n is the column height after *n*-cycles of intermittent MAGE; 1, 2, ..., *n* and 1′, 2′, ..., *n′* correspond to the on- and off-cycles, respectively, in each complete cycle; R_{max} and R_{min} represent the maximal and minimal radii of the column corresponding to the points with the highest (E_{max}) and the lowest strength (E_{min}) in each intermittent cycle. (b) Distribution map of the electric-field strength simulated with the software ANSYS 8.0 for the system conducted by intermittent MAGE at the final stage. The bias is 3.2 V and the conductivity of the electrolyte is 42.02 mS cm^{-1}

simulate the continuous MAGE conducted in different conditions. Diagrams were constructed and the data of ΔE^c and E_m^c were evaluated and compared. In a system where the microanode ascended at 2 μm s^{-1}, the profile of the microcolumn is determined by the electric voltage. The relationship between the surface morphology of the microcolumns and the voltage is discussed later in terms of ΔE^c and E_m^c.

6. Models for column growth in intermittent MAGE

Figure 8(a) shows the schematic models for the intermittent MAGE process. The microanode was first ascended to keep an initial separation of 10 μm from the substrate, and the power was turned on to proceed electrochemical reaction at a certain voltage. This electroplating process was carried out until the microcolumn growing up to almost in contact with the microanode, as shown at stage 1. The power was switched off to interrupt the electrochemical reaction, the microanode was ascended to another gap (at 10 μm), as depicted in stage 1′. Monitoring of the current would provide with a criterion for this on/off decision-making. The power would keep on as the current measured is less than 20 mA; however, it would turn to off as the current is higher than 20 mA. Another gap of 10 μm-gap was set and the second cycle would succeeded to undergo stages 2 and 2′, and so on until the nth cycles (via stages n and n′) to accomplish a microcolumn with an overall height of hn. It is apparent that microcolumn revealed a periodic variation in radius (from R_{min} to R_{max} and R_{min} again) in response to periodic performance of the intermittent MAGE through positions $E_{max}^{(n-1)}$ to E_{min}^n and E_{max}^n again. It is worth noting that the mean strength of electric field (i.e., E_m^i) can be calculated from two different positions (i.e., E_{max}^n and E_{min}^n) in Eq. (6.1) as follows

$$E_m^i = \left[E_{min}^n + E_{max}^n \right] / 2 \tag{6.1}$$

$E^i{}_m$ may offer a criterion to predict whether the microcolumn keeps on growing. In addition, the strength difference (i.e., ΔE^i) of the electric field between positions E_{max}^n and E_{min}^n can be estimated in Eq. (6.2) in the following

$$\Delta E^i = E_{max}^n - E_{min}^n \tag{6.2}$$

ΔE^i may offer an estimation of the diameter uniformity for the column fabricated from intermittent MAGE.

Figure 8(b) shows a schematic diagram to elucidate the distribution of the electric field in the intermittent MAGE conducted at an electric bias of 3.2 V, with the initial gap of each intermittent cycle at 10 μm. This diagram was also established via simulation by using commercial software ANSYS 8.0 through input the data of electrical conductivity for the electrolyte. A number of diagrams were constructed depending upon various experimental parameters and the corresponding data of E_m^i and ΔE^i were evaluated. The relationship between the surface morphology and the electric voltage employed in the intermittent MAGE is discussed later on basis of E_m^i and ΔE^i data.

7. Effect of electric voltages on the surface morphology and radius of the microcolumns

Figure 9 shows the effect of the electric voltages on the average radius (to the left ordinate) of the microcolumns fabricated from continuous MAGE. The radius of the columns was

evaluated from the SEM micrographs. The average radius was calculated from arithmetic average of three microcolumns fabricated under the same conditions. Standard deviation of the data was concerned in the plot. The average radius of the microcolumns tended to increase gradually from 2.59 to 10.34 μm with increasing the voltage from 1 to 5 V; however, it increases suddenly from 10.34 to 26.77 μm with increasing the voltage form 5 to 6 V. The standard deviation of the radius increases from 1.54 to 3.11 μm in the range from 1.0 to 4.0 V but decreases from 3.11 to 0.77 μm in the range from 4.0 to 6.0 V. At voltages below 5 V, a short vertebra-like structure was slowly formed to reveal a smaller radius at the top. When the continuous MAGE conducted in the range from 5 to 6 V, the growth rate of the micro-feature seemed to be similar to the ascending rate of the microanode. This led to a longer microcolumn appearing in uniform diameter.

Figure 9 also depicts the dependence of the mean strength (E_m^c , to the right ordinate) on the electric voltages. The magnitude of E_m^c almost increases one order of magnitude with increasing the voltage from 1.0 to 5.0V, and roughly 50 times with an increase of voltage from 5.0 to 6.0 V. A sudden rise in E_m^c within the range from 5.0 to 6.0 V is ascribed to much higher growth rate of the column compared to the ascending rate of the microanode. In practice, the huge change in E_m^c may lead to a problem to balance the growth rate and the ascending rate between the microcolumn and microanode.

Variation of ΔE^c with the voltages applied in continuous MAGE is also of concern. It reveals gradual increase (from 37 to 1238 V m^{-1}) with increasing the voltage from 1 to 5 V; however, a sudden increase (from 1238 to 140 000 V m^{-1}) within 5 –6V. The gradual increase of ΔE^c results in a radius discrepancy of the cylinder-like column with the voltages within 1 – 5 V. The sudden rise of ΔE^c tends to a momentary growth of the micro feature thus leading to rapid touch with the microanode. Thus, conducting continuous MAGE within 5–6 V to fabricate microcolumns is impractical.

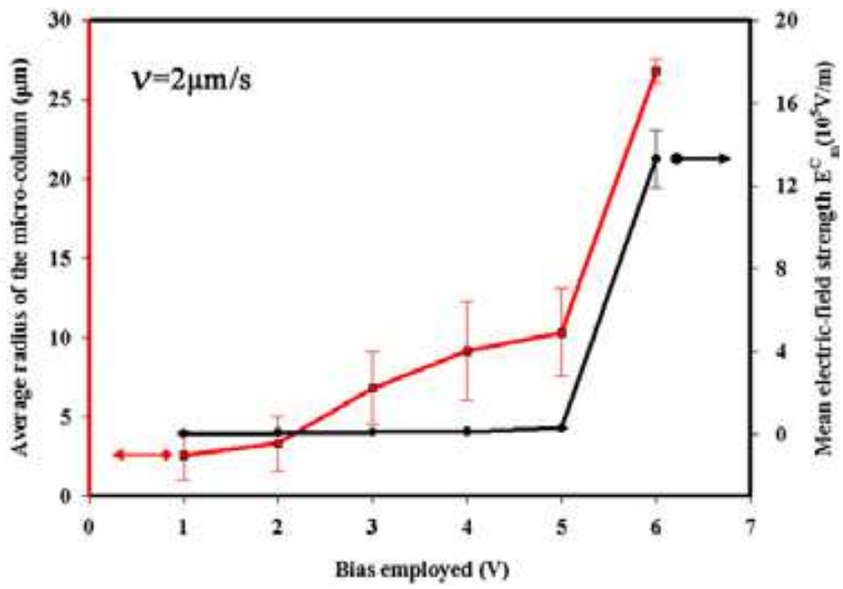

Fig. 9. Variation of the average radius for the micrometer columns (left ordinate) and the mean strength of the electric field (right ordinate) with the bias employed in the process of continuous MAGE with various ascending rates of the microanode in 240 s. The initial separation between the microanode and the Cu-substrate was 20 μm

Figure 10 depicts the dependence of the column radius (to the left ordinate) upon the voltages employed in the intermittent MAGE. The radius increases gradually (from 22.20 to 31.23 μm) with increasing the voltages from 3.2 to 4.2 V, and so does the corresponding standard deviation (from 0.25 to 1.75 μm.)

Regarding the dependence of the mean strength (E_m^i) of electric field (to the right ordinate) upon the voltages applied in the intermittent MAGE. The mean strength displays a gradual increase from 194 324 to 268 163 V m^{-1} (roughly 1.4 times) in the range from 3.2 to 4.2 V. The gradual change of E_m^i reflects the availability to manipulate experimental conditions in fabrication of the columns. The microcolumns fabricated at higher voltages depict greater standard deviation. This result reflects high degree of non-uniformity for the columns fabricated at higher voltages. Checking the data of ΔE^i (increase from 9909 to 37 391 V m^{-1}), the result is consistent. A comparison is made for fabricating microcolumns by means of intermittent MAGE (in the range from 3.2 to 4.2 V) and continuous MAGE (in the range from 5.0 to 6.0 V). Strength change in the electric field and standard deviation from the mean strength is much higher in the continuous MAGE than in the intermittent MAGE. Due to this fact, intermittent MAGE is better than continuous MAGE to fabricate microcolumn with a uniform diameter at expected length.

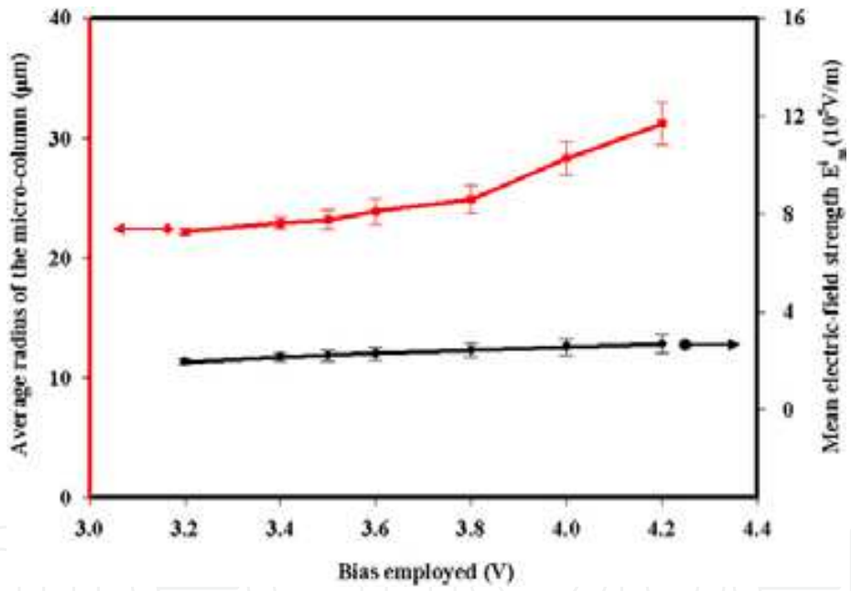

Fig. 10. Variation of the average radius for the micrometer columns (left coordinate) and the mean strength of the electric field (right coordinate) with the bias employed in the process of intermittent MAGE to a height of 500 μm. In each intermittent cycle, a gap of 10 μm is set between the microanode and the top of the column.

8. Surface and transverse morphology of micrometer columns influenced by electrical voltages

Micrometer nickel columns obtained from intermittent MAGE were treated in the following procedures to observe their cross section. They were first mounted in an epoxy resin. The mounted columns were ground in a plane perpendicular to the longitudinal direction to expose their cross-sections. A series of carbide paper (in the grade of 400, 600, 800, 1000,

1200, 2000) were used in the wet grinding, and subsequently slurries with fine powders of Al_2O_3 (1.0 and 0.3 μm in diameter, respectively) were employed to polish the cross-sectional surface to a mirror. The mirror surface was pickled in a 0.1% HF solution for 30 s, rinsed with water and dried ready for the SEM examination. Figure 11 displays the SEM morphologies and their transverse section at the position marked with a line across the micrometer. Ni columns deposited at 3.2V (Fig. 11(a)), 3.4V (Fig. 11(b)), 3.6 V (Fig. 11(c)), 4.4 V (Fig. 11(d)) and 4.6 V (Fig. 11(e)). Obviously, the surface morphology and transverse structure of the columns revealed a big difference depending on the biases. The micrometer columns deposited at 3.2 V depicted a smooth surface and a regular circular transverse (Fig. 11(a)). Checking the micrographs shown in Fig. 11 (from 11(a)–(e)),we found that by increasing the electrical voltages, the columns grew into shapes with higher irregularity and less smoothness on their surface. The columns deposited at higher voltages (e.g., 4.4 V) displayed an uneven circular profile around the transverse with the surface in nodular morphology. The columns deposited at much higher voltages (e.g., 4.6 V) appeared to have a branched coral with irregular transverses shape. We were concerned with the internal compactness of the columns, which could be estimated by examining their transverse using the SEM. The compactness was found to vary to different extents, depending on the electrical biases employed. Full compactness was observed in the transverse of the columns deposited at 3.2 V (Fig. 11(a)). Less compact were the columns, with porosity in the center of their transverse (Fig. 11(c)), deposited at little higher voltages (e.g., 3.6 V). The compactness was much less for the columns (Fig. 11(c)) deposited at much higher voltages (e.g., 4.4 V), because of radial expansion of the porosity from the transverse center resulting from coarsening and combination of the voids. The interior of the transverse was almost empty and remained a coral shell for the columns fabricated at an extremely high voltage (i.e. 4.6V). The deposit looked like a branched coral with a hollow interior.

9. Local potential measurement

Figure 12 depicts the scheme of an experimental setup for conducting LECD by a MAGE system. The microanode was driven to move by a step motor through an interface controlled by a computer, and the electroplating current was measured using a galvanometer. In addition, we set up a microelectrode, coupled with the saturated calomel electrode in connection with a potentiostat (Princeton EG&G Model 273 A), to oversee the potential at the location where the LECD proceeded. At least three runs had been carried out, and the standard deviation was presented in the error bar. Before setting out the deposition, the open-circuit potential was recorded (i.e. at -491.0 mV versus the SCE). The microanode was descended to touch the cathode, then drawn back to keep an initial gap at 10 μm to start the intermittent MAGE process as mentioned earlier. Once the power switched on, the potential decreased suddenly within several tenths of a second and level off to different levels depending on the electric voltages applied. This potential drop implies the occurrence of electroplating and the deposition rate could be estimated from the magnitude of current. Variation of the current with time has been discussed so we concentrate on the local potential in this section.

Figure 13 depicts the variation of local potential in the intermittent MAGE process against the voltages. Prior to electrochemical deposition, the open circuit potential (OCP) was stabilized at -491.0 mV. It dropped suddenly to a variety of levels in few tenths of a second once the electroplating setting out. The potential level decreased (in the range from -550.0 to -635.0 mV) with increasing the voltages from 3.2 to 4.6 V. The difference between the OCP

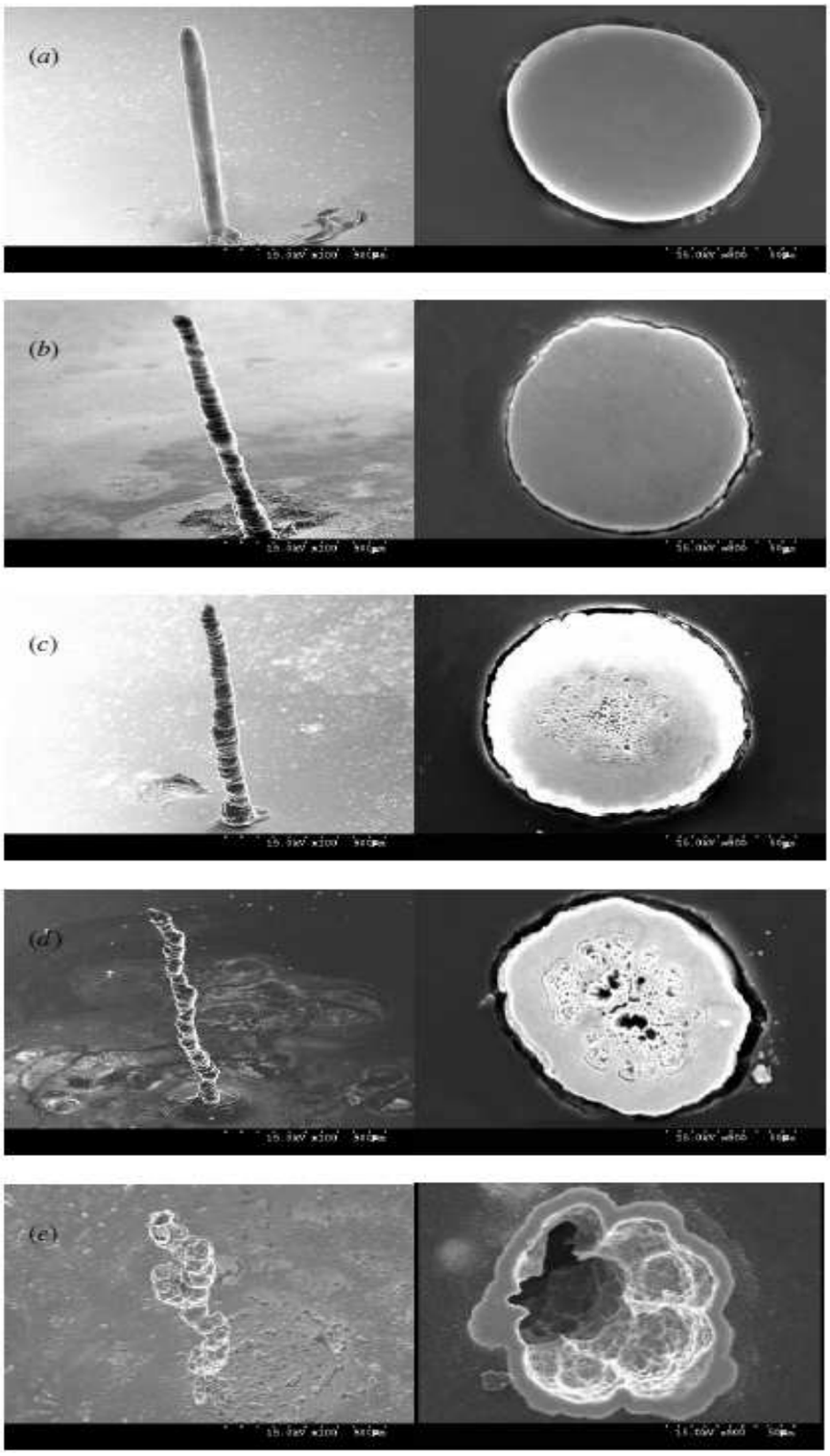

Fig. 11. SEM morphologies for the micrometer Ni columns deposited at various voltages and their corresponding transverse section. The columns were deposited at (a) 3.2V,(b) 3.4 V, (c) 3.6 V, (d) 4.4V and (e) 4.6 V with the gap between the electrodes initially set at 10 μm

and local potential measured under various voltages was of concern. The difference is much greater (i.e. 144.0 ± 1.0 mV) for the MAGE conducted at 4.6 V than that (59.0 ± 1.0 mV) conducted at 3.2 V.

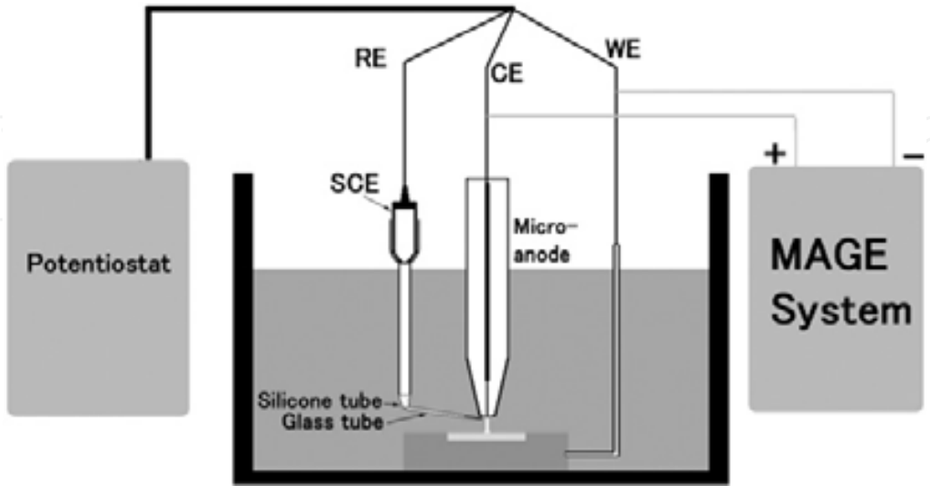

Fig. 12. Schematic diagram of the experimental setup for LECD conducted with the MAGE system and the local potential at the location near the top of the micrometer column measured by a microelectrode coupled with the SCE connected with a potentiostat

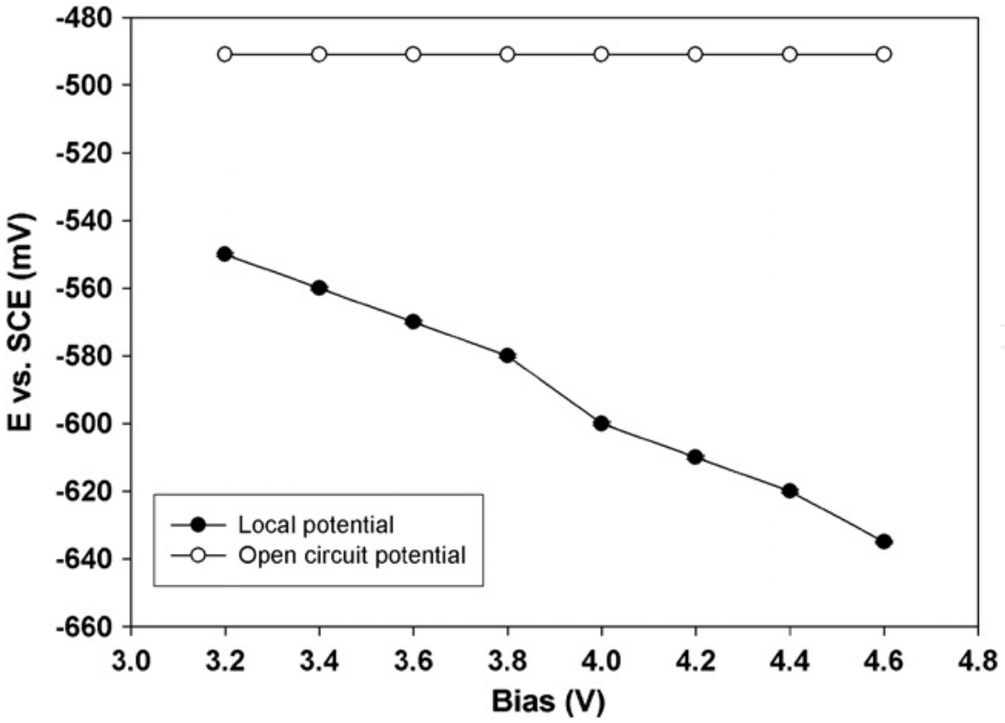

Fig. 13. A plot of open-circuit potential and local potentials against the voltages employed in the MAGE with the initial gap at 10 μm between the electrodes

10. Average growth rate for the columns with a height of 1000 μm

Figure 14 shows the dependence of the average growth rate (in the right ordinate) on the voltages employed to grow a micrometer Ni column, 1000 ± 10 μm in height. The average growth rate was calculated by dividing the height of the columns (i.e. 1000 ± 10 μm) by the growth duration. The time taken by the step motor should be deducted from the total duration of the process. From Fig. 14, the growth rate at 3.2 V is 0.114 μm s^{-1} and it increases from 0.114 ± 0.004 to 1.76 ± 0.06 μm s^{-1} with increasing the voltages from 3.2 to 4.6 V. The standard deviation increases with an increase of voltages. Voltages less than 3.2 V or higher than 4.6 V were ignored because of impractical tiny rate in the former and unsatisfactory appearance for the deposits obtained in the latter. In Fig. 14, the average current responsible for LECD was also measured and plotted (in the left ordinate) against the voltages. It increases from 0.225 ± 0.021 to 1.881 ± 0.046 mA with increasing the voltage from 3.2 to 4.6 V. The current is almost nine fold for the MAGE conducted at 4.6 V in comparison to that at 3.2 V. With respect to error bars in Fig. 14, the standard deviation increases with voltages. The growth rate estimated from the data of average current is consistent with that evaluated from column height divided by the electroplating duration.

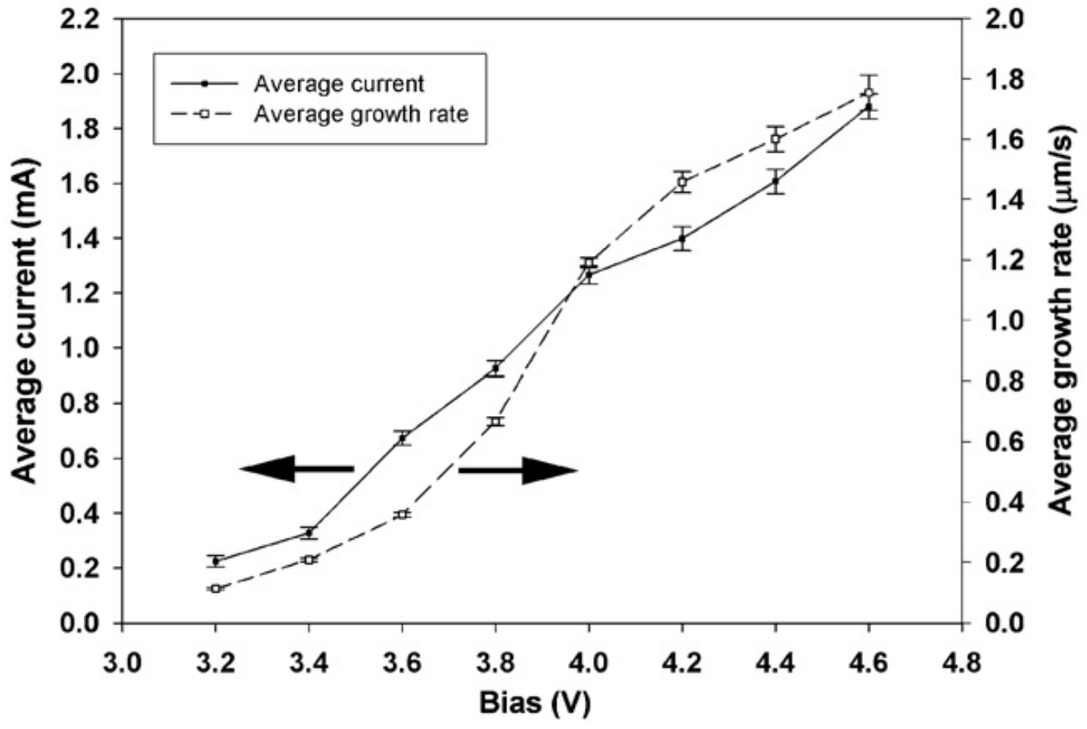

Fig. 14. A plot of the average current and average growth rate for the columns against the electrical bias employed in the MAGE

11. Concentration of nickel ions in the location proceeding LECD

As shown in Fig. 14, the stabilized local potential was in the range from -550 to -635 mV for the intermittent MAGE conducted at voltages ranging from 3.2 to 4.6V (vs. SCE). The

concentration of nickel ions at the local site taking place LECD could be estimated by the Nernst equation as shown in the following.

$$E = E^0 + \frac{RT}{\nu_e F} \ln\{c_{ox} / c_{Red}\} \tag{11-1}$$

Where E^0 is the standard potential of the electrode, R is gas constant, T is absolute temperature, ν_e is the valence number of the metal and F is Faraday's constant. C_{ox} and C_{Red} are the concentrations of oxidation species and reduction species.
By substituting E^0 with -0.25V (i.e. the standard EMF for 1.0 M nickel ions [12]), T with 328 K (55°C), R with 8.3144 joules/degree-mole (gas constant), F with 96487 Coulomb/mole and ν_e = 2, we gained the equation against SHE as follows.

$$E = -0.491 + \frac{0.065}{2} \log\left\{Ni^{2+}\right\} \quad \text{VS.} \quad \text{SHE} \tag{11-2}$$

In place of E in equation (11-2) with the data of local potentials measured under various voltages, the steady-state concentration of nickel ions remained at the location after LECD can be calculated. The concentration of nickel ions is plotted against the voltages employed in intermittent MAGE, as shown in Fig. 15. It reveals nickel ions remaining in the LECD vicinity decrease suddenly when increasing the voltages from 3.2 to 4.6 V.

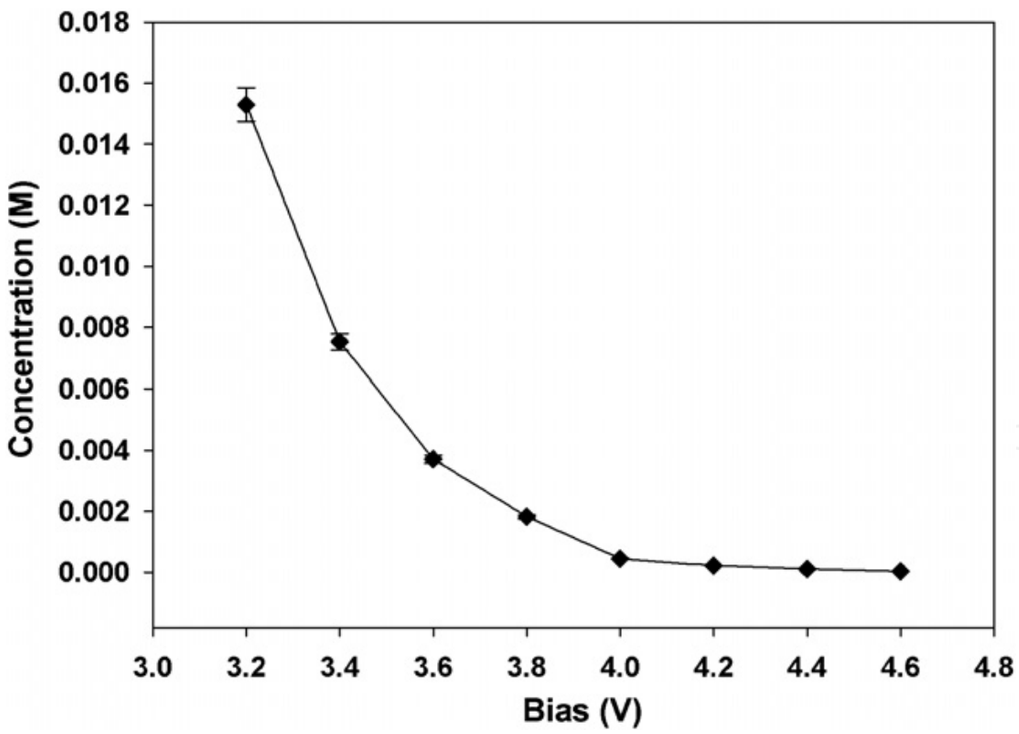

Fig. 15. The concentration of nickel ions calculated from stabilized local potentials at the location where the LECD takes place

A blank test was carried out to verify the correspondence between the electric potential and the concentration of nickel ions present in the solution. The bath conditions were set

unchanged except the concentration of nickel ions. The potential was measured using the same reference microelectrode depicted in Fig. 12. The relationship between the potential measured and the concentration of nickel ions prepared was plotted in Fig. 13. The curve representing the dependence of potential on the concentration of nickel ions obeyed equation (11-2) is in good agreement with that based on experimental measurements.

12. Supply of nickel ions from bulk solution to the LECD location

Mass transport of nickel ions in the electroplating process is theoretically governed by the Nernst-Planck equation [13]. According to the Nernst-Planck equation, the flux (in mol s^{-1} m^{-2}) for the specific ions transported and to be deposited (assigned as J_i) is represented as

$$J_i = -D_i \nabla C_i - \frac{Z_i F}{RT} D_i C_i \nabla \phi + C_i v \tag{12-1}$$

Where D_i is the diffusion coefficient (in m^2 s^{-1}), ∇C_i is the concentration gradient, $\nabla \phi$ is the potential gradient, Z_i and C_i are the charge (dimensionless) and concentration (in mol m^{-3}) of species i, respectively, and v stands for the velocity (in m s^{-1}) of the solution flow under stirring. In equation (12-1) the flux is expressed in detail with three terms on the right-hand side to describe the contribution of diffusion, migration, and convection, respectively. The diffusion coefficient (D_i) of nickel ions in the solution is 8.157×10^{-10} m^2 s^{-1} [14]. The concentration of nickel ions in the bulk solution of watts bath is 1.445×10^3 mol m^{-3}. The convection term in Equation (12-1) could be ignored in the LECD process without stirring.

In an attempt to calculate the flux of nickel ions transported in the LECD process, the geometric transport in a specific electric field should be considered. As soon as the voltages are applied, nickel ions nearby the electrodes migrate to the cathode surface to discharge and are consumed. Reduction of nickel ions into metallic nickel within the local region leads to depletion of the nickel ions. This depletion causes a concentration gradient as compared this location to the around surroundings. The gradient offers a driving force for diffusion of nickel ions from the bulk solution to the depletion zone. Neglecting the initial stage in LECD, the micrometer columns are steadily deposited in an egg-head on their top [15]. We presume the nickel ions migrate into a boundary of semi-sphere rather than egg-head for simplifying the calculation. The semi-spherical boundary responsible for migration is illustrated in Fig. 16a. The nickel ions discharge and are consumed in the electric field surrounded with a cone. The boundary of the cone responsible for further supply of nickel ions by diffusion is illustrated in Fig. 16b. In Fig. 16, r is the average radius (in m) of the microcolumn, g marks the gap (also in m) between the microanode and the top of the column deposited. The area for the semi-sphere (A_{mig}, in m^2) and for the cone (A_{diff}, in m^2) can be estimated in the following:

$$A_{mig} = 2\pi r^2 \tag{12-2}$$

$$A_{dif} = 2\pi(r+g)\left(\frac{125\times10^{-6}/2 + r}{2}\right) \tag{12-3}$$

The figure 125 x 10^{-6} in equation (12-3) is the diameter of the tip-end disk of the microanode. The extent of r can be evaluated through examining the columns with SEM, and g is replaced by 10^{-5} m in this work because of its initial setting.

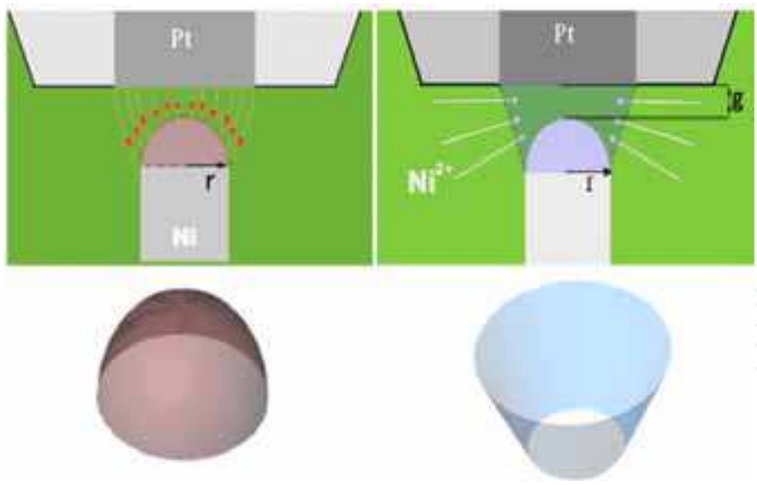

Fig. 16. Schematic models to illustrate the region involving mass transportation of nickel ions caused by (a) migration and (b) diffusion

The transport rate of nickel ions to the location exerted LECD can be arrived at from a product between the flux and the area of the plane perpendicular to the transport direction.

$$Transport\ rate(mol/s) = J(mol/s \cdot m^2) \times A(m^2) \tag{12-4}$$

An instance is given to explain calculating the fluxes for the transport of nickel ions by migration and diffusion, respectively, in the process performed at 3.2 V.

$$J_{mig} = -\frac{2 \times 96487}{8.314 \times 328} \times 8.157 \times 10^{-10} \times C_{local} / 10^{-3} \times \frac{voltage}{10 \times 10^{-6}} \tag{12-5}$$

$$J_{dif} = -8.157 \times 10^{-10} \times \frac{(1.445 - C_{local}) / 10^{-3}}{r \times 10^{-6}} \tag{12-6}$$

Replacing the voltage in equation (12-5) with 3.2 V, C_{local} in equation (12-6) with the value read from Fig. 15 (i.e., 0.01530 M), and r with the radius (that is, 36.1μm) of columns measured in the SEM micrograph, we obtain the fluxes of nickel ions contributed by migration and diffusion separately as follows.

$$J_{3.2Vmig} = -\frac{2 \times 96487}{8.314 \times 328K} \times 8.157 \times 10^{-6} \times 0.01530 mol/L \times 3.2V / 10\mu m \tag{12-7}$$

$$J_{3.2Vdif} = -8.157 \times 10^{-6} cm^2/s \times \frac{(1.445 - 0.01530) mol/L}{36.1\mu m} \tag{12-8}$$

From equation (12-4), we can estimate the total transport using equation (12-9)

$$Transport\ rate_{total} = J_{dif} \cdot A_{dif} + J_{mig} \cdot A_{mig} = 2.77 \times 10^{-9} mol/s \tag{12-9}$$

The same treatment can be used to calculate the corresponding transport rate for the LECD performed under other voltages. The average supplying rate calculated from equation (12-9) is plotted with the voltages, as shown in Fig. 17.

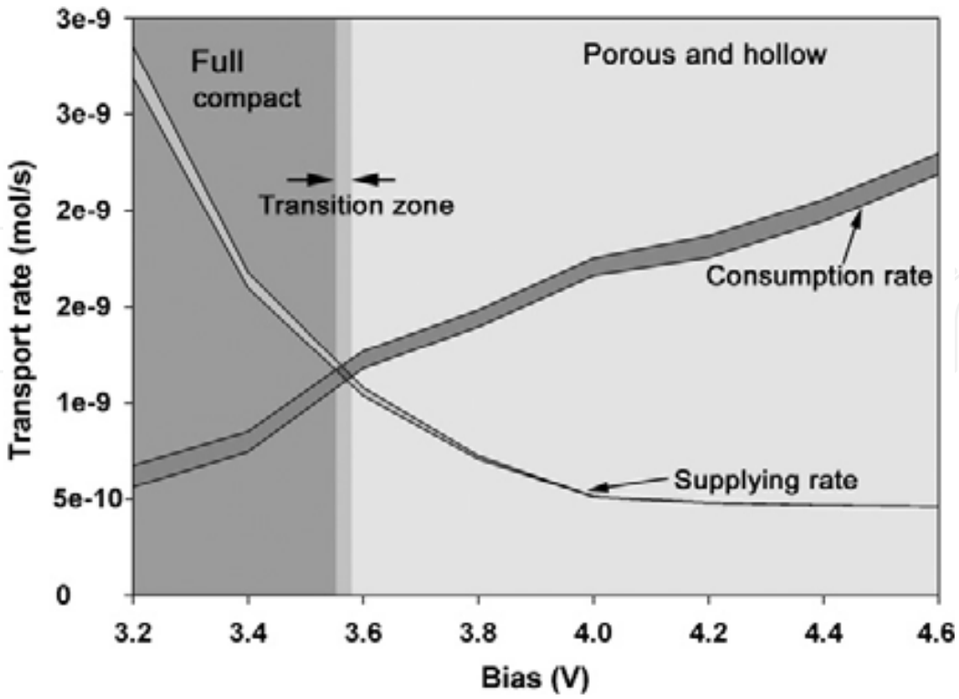

Fig. 17. Transport rate as a function of voltages adopted in the intermittent MAGE to display the balance between the supply and consumption rate of the nickel ions within the localization taking place LECD

13. Consumption of nickel ions in the LECD location

Figure 18 displays the plot of average current measured at steady state in the LECD and the current efficiency against the voltages employed. It is seen in Fig. 18 the average current increases from 0.2 to 1.8 mA, whereas the current efficiency decreases from 53 to 23 % with increasing the biases in the range from 3.2 to 4.6 V. The standard deviation of the average current also increases with the electrical biases. Observation suggested the increase in average current is proportional to the augmenting in the growing rate of columns. The decrease in the current efficiency responds to the phenomenon that bubbles evolve much more generously when increasing the biases. This enlargement in bubbles evolution implies reducing hydrogen ions contributes much more than nickel ions. The higher standard deviation in the average current at higher corresponding biases reflects the greater variation in the diameter of the columns and in the roughness of their surface morphology.

The weight of a single micrometer column is so slight and beyond the detection limit of a usual balance. Three columns fabricated at the same conditions were gathered to overcome this difficulty, thus an average weight for a single column could be estimated ($W_{estimated\ by\ weighing}$). The current efficiency (η) for the LECD conducted under specific conditions can be estimated by equation (13-1)

$$\eta = \frac{W_{estimated\ by\ weighing}}{W_{calculated\ from\ current}} \tag{13-1}$$

In which the numerator ($W_{estimated\ by\ weighing}$) is the average weight obtained by the aforementioned for a single micrometer column and the denominator ($W_{estimated\ by\ weighing}$) was

calculated from the data of electroplating current consumed to grow the column within the duration. The theoretical weight of the column ($W_{estimated\ by\ weighing}$) estimated by the data of current and duration measured is believed to obey the following equation (13-2).

$$W_{calculated\ from\ current} = \frac{ItA}{zF} \tag{13-2}$$

Where I is the average current; t is the duration to grow a 1000 μm-height column; A is the atomic weight of nickel; z is the valence; and F is the Faraday constant. The average consumption rate of the nickel ions in the local region taking place by LECD could be estimated by the equation (13-3)

$$\text{Consumption } rate = \frac{W}{t \times A} = \frac{I\eta}{zF} \tag{13-3}$$

The average consumption rates calculated from equation (13-3) are plotted with the voltages, as shown in Fig. 17

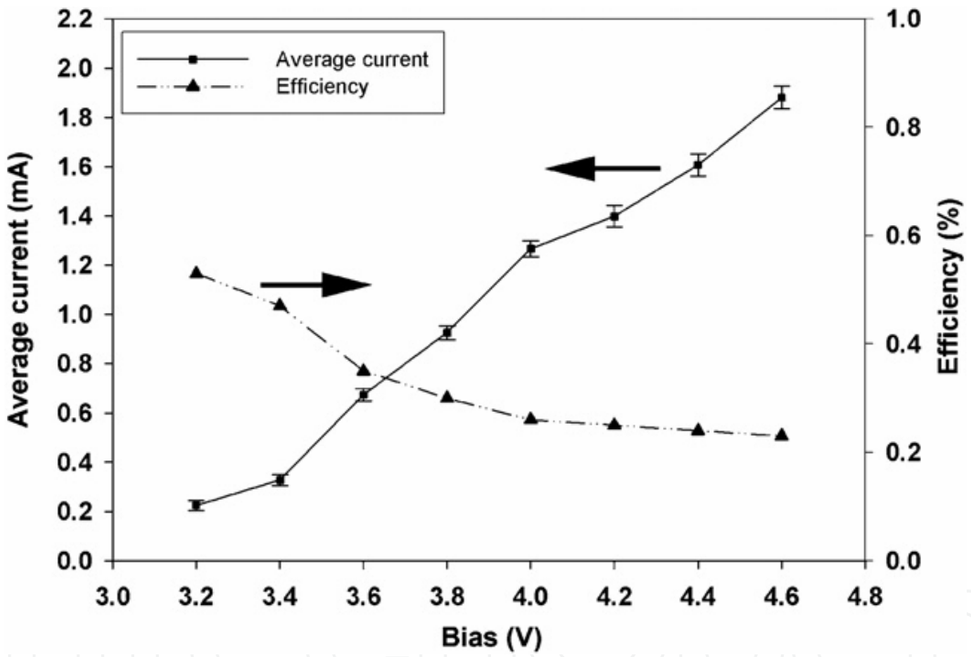

Fig. 18. The average current measured in the LECD and the current efficiency plotted against the electrical bias (voltage) employed

14. Balance between the supply and consumption of nickel ions within the location taking place LECD

Figure 17 summarizes the variation of supply rate and consumption rate within the location where taking place LECD with the voltage employed in the intermittent MAGE. The increase in the consumption rate and the decrease in the supply rate when increasing the electrical biases tend to meet at a point which reaches a balance. At the balance point the consumption rate of nickel ions in the local region could be compensated by the supply rate. Therefore, this point defines a critical voltage to separate the columns with internal

transverse in compact from those with porous transverse internal. At voltages less than the critical, the columns will lead to a compact transverse, whereas at voltages higher than the critical the columns will lead to a porous one. Considering the LECD performed at 3.2V the supplying rate of nickel ions (that is, 2.77 $x10^{-9}$ mol s^{-1}) is much higher than the consumption rate (that is, 6.19 $x10^{-10}$ mol s^{-1}). Nickel ions supplied to the location are more than consumed within the LECD region. Surplus supply of nickel ions leads to a complete filling of internal transverse of the columns. Stable current results in smooth morphology of the columns. On the other hand, as the LECD performed at 4.6V, the supply rate (4.58 $x10^{-10}$ mol s^{-1}) is much less than the consumption rate (2.24 $x10^{-9}$ mol s^{-1}). Shortage of nickel ions resultant from a lower rate of supply rate than the consumption leads to formation of internal pores thus resulting in porous transverse in the center of the columns. Greater variation in the deposition current results in rough morphology of the columns. The higher the biases employed in the LECD, the more severe the porous transverse in the columns, and the rougher their surface, as shown in Fig. 11.

There exists a transition zone in a narrow range of the electric bias (from 3.55 to 3.57 V) in Fig. 17. This transition zone arises from the deviation of accuracy in calculating of nickel concentrations and measuring local potentials. Apparently, the accuracy deviation is so small (at 0.02 V) that 3.56 ± 0.01 V is the critical voltage for conducting the intermittent MAGE to separate the micrometer columns with a smooth surface and full compact internal from those with rough surface and porous (or even hollow) internal. At any voltage less than this critical, the nickel ions consumed by electrochemical deposition in the depletion region could be completely compensated by the diffusion of nickel ions from nearby surroundings. This ensures sufficient supply for the need in the electrochemical consumption thus resulting in a full compact internal transverse of the columns. On the contrary, at the overages higher than this critical, the consumption of nickel ions is faster than their supply within the electroplating location. Insufficient supply of nickel ions leads to a porous (and even empty) internal transverse of the columns. Lower current density arising from the cases conducted at lower voltages results in a finely grained smooth surface; higher current density arising from the cases conducted at higher voltage results in an irregularly nodular rough surface.

15. Conclusions

The kinetics of electrochemical processes is determined not only by the strength of electric field but also by the mass transport phenomenon of the electrochemical active ions. In the cases of ordinary electrochemical deposition, the electric field employed is relatively low and the field distribution is homogeneous. Localized electrochemical deposition (LECD) process provides a new concept to fabricate three-dimensional (3D) metal microstructures. However, a super high electrical field is exerted at the electroplating site in the LECD, and the distribution of field strength is ultra heterogeneous. The site chosen to conduct LECD is controlled experimentally to follow the track guided with a microanode. Consequently, LECD is also named as microanode guided electroplating (MAGE) process.

Through discussion on the phenomenon of mass transport in such a strong field distributed in extremely heterogeneous manner, balance between the supply rate and consumption rate of nickel ions in the region where LECD taking place plays a role on the surface morphology and the transverse internal structure. This balance is determined significantly by experimental parameters such as motion modes of the microanode, applied electric voltage, initial gap between the cathode and microanode. In terms of models, we simulate the system with commercial software ANSYS 8.0 to realize the electrochemical mechanism satisfactory.

16. Acknowledgments

The authors are grateful to the National Science Council of the Republic of China (Taiwan) for the financial support of the project under contract No. NSC 97-2221-E-008-009-MY3.

17. References

[1] J. D. Madden and I. W. Hunter, "Three-dimensional micro fabrication by localized electrochemical deposition", *J. Micromech. Microeng*., 1996, 5, 24–32.

[2] J. C. Lin, S. B. Jiang, D. L. Lee, C. C. Chen, P. C. Yeh, T. K. Chang, J. H. Yang, "Fabrication of micrometer Ni columns by continuous and intermittent microanode guided electroplating", *J. Micromech. Microeng*. , 2005, 15, 2405–2413.

[3] D. L. Lee, J. C. Lin, P. F. Kao, S. B. Jiang, "Micro-anode Guided Electroplating (MAGE) control system", *Materials Science Forum*, 2006, 505~507, 115-120.

[4] T. K. Chang, J. C. Lin, J. H. Yang, P. C. Yeh, D. L. Lee and S. B. Jiang, " Surface and transverse morphology of micrometer nickel columns fabricated by localized electrochemical deposition", *J. Micromech. Microeng*. 2007, 17, 2336–2343.

[5] J. H. Yang, J. C. Lin, T. K Chang, G. Y. Lai and S. B. Jiang, "Assessing the degree of localization in localized electrochemical deposition of copper", *J. Micromech. Microeng*., 2008, 18, 055023 -005030.

[6] J. C. Lin, T. K. Chang, J. H. Yang, J. H. Jeng, D. L. Lee and S. B. Jiang, "Fabrication of a micrometer Ni–Cu alloy column coupled with a Cu micro-column for thermal measurement", *J. Micromech. Microeng*., 2008, 19, 015030-015039.

[7] J. H. Yang, J. C. Lin, T. K. Chang, X. B. You and S. B. Jiang, "Localized Ni deposition improved by saccharin sodium in the intermittent MAGE process", *J. Micromech. Microeng*., 2009, 19, 025015-25026.

[8] J. C. Lin, J. H. Yang, T. K. Chang, H. B. Jiang, "On the Structure of Micrometer Copper Features Fabricated by Intermittent Microanode-guided Electroplating", *Electrochim. Acta*, 2009, 54, 5703-5708.

[9] J. C. Lin, T. K. Chang, J. H. Yang, Y. S. Chen, and C. L. Chuang, " Localized Electrochemical Deposition of Micrometer Copper Columns by Pulse Plating", *Electrochim. Acta*, 2010, 55 , 1888-1894.

[10] Ting-Chao Chen, Yean-Ren Hwang, Jing-Chie Lin, Yong-Jie Ciou, "The Development of a Real-Time Image Guided Micro Electroplating System", *Int. J. Electrochem. Sci*., 2010, 5, 1810 - 1820.

[11] Y. S. Chen, J. C. Lin, Z. H. Lin, C. Li, and J. K. Chang, "Effect of Solvent on the Morphology of Nickel Localized Electrochemical Deposition", *J. Electrochem. Soc*., 2011, 158 (5) D264-D268.

[12] D. A. Jones, "Principles and Prevention of Corrosion", 2nd Edn. Englewood Cliff, NJ: *Prentice Hall*. 1996, 44

[13] A. J. Bard and L. R. Faulkner, "Electrochemical Methods Fundamentals and Applications", 2nd Edn., New York: *Wiley*, 2000, 29

[14] D. R. Lide, 2001–2002 CRC, "Handbook of Chemistry and Physics", 82nd Edn., Boca Raton, FL: CRC Press.

[15] K. Ikuta, S. Maruo and S. Kojima, " New micro stereo lithography for freely movable 3D micro structures", *J. Microelectromech. S*. 1998, 290–2955

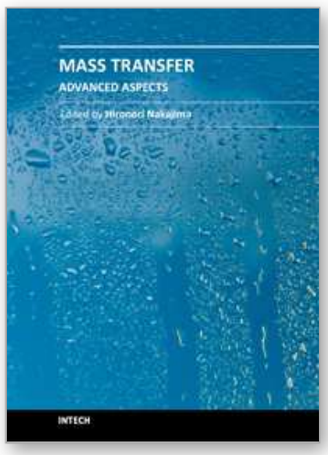

Mass Transfer - Advanced Aspects

Edited by Dr. Hironori Nakajima

ISBN 978-953-307-636-2
Hard cover, 824 pages
Publisher InTech
Published online 07, July, 2011
Published in print edition July, 2011

Our knowledge of mass transfer processes has been extended and applied to various fields of science and engineering including industrial and manufacturing processes in recent years. Since mass transfer is a primordial phenomenon, it plays a key role in the scientific researches and fields of mechanical, energy, environmental, materials, bio, and chemical engineering. In this book, energetic authors provide present advances in scientific findings and technologies, and develop new theoretical models concerning mass transfer. This book brings valuable references for researchers and engineers working in the variety of mass transfer sciences and related fields. Since the constitutive topics cover the advances in broad research areas, the topics will be mutually stimulus and informative to the researchers and engineers in different areas.

How to reference

In order to correctly reference this scholarly work, feel free to copy and paste the following:

Jing-Chie Lin, Ting-Kang Chang, Jen-Horn Yang, Yean-Ren Hwang and Chuan Li (2011). Mass Transfer Within the Location Where Micro Electroplating Takes Place, Mass Transfer - Advanced Aspects, Dr. Hironori Nakajima (Ed.), ISBN: 978-953-307-636-2, InTech, Available from: http://www.intechopen.com/books/mass-transfer-advanced-aspects/mass-transfer-within-the-location-where-micro-electroplating-takes-place

INTECH
open science | open minds

InTech Europe
University Campus STeP Ri
Slavka Krautzeka 83/A
51000 Rijeka, Croatia
Phone: +385 (51) 770 447
Fax: +385 (51) 686 166
www.intechopen.com

InTech China
Unit 405, Office Block, Hotel Equatorial Shanghai
No.65, Yan An Road (West), Shanghai, 200040, China
中国上海市延安西路65号上海国际贵都大饭店办公楼405单元
Phone: +86-21-62489820
Fax: +86-21-62489821

IntechOpen